BBA - General Subjects 1863 (2019) 893–902

Contents lists available at ScienceDirect

BBA - General Subjects

journal homepage: www.elsevier.com/locate/bbagen

Monitoring Caco-2 to enterocyte-like cells differentiation by means of electric impedance analysis on printed sensors

Marziano M.[a,b,*], Tonello S.[a], Cantù E.[a], Abate G.[b], Vezzoli M.[b], Rungratanawanich W.[b], Serpelloni M.[a], Lopomo N.F.[a], Memo M.[b], Sardini E.[a], Uberti D.[b]

[a] Department of Information Engineering, University of Brescia, Brescia, Italy
[b] Department of Molecular and Translational Medicine, University of Brescia, Brescia, Italy

ARTICLE INFO

Keywords:
Caco-2 cells
Barrier integrity
Cell differentiation
Enterocyte-like cells
Impedance-based sensors

ABSTRACT

Background: Colorectal adenocarcinoma cells (Caco-2) are a widely used model of intestinal barrier to study cancer development, toxicological assessments, absorption and metabolism in food science or drug discovery. Caco-2 spontaneously differentiate into a monolayer expressing several specific characteristics, typically showed by mature enterocytes. For in vitro experiments, it is crucial to identify non-invasive and non-destructive techniques able to evaluate the integrity and differentiation of the cells monolayer. Thus, we aimed to assess these properties by analyzing electrical impedance measurements.

Methods: Caco-2 cells were differentiated for 21 days. The monolayer integrity and differentiation were primarily evaluated by means of morphological, biochemical and molecular data. Impedance measurements in a range of frequencies from 400 Hz to 50 kHz were performed using a dedicated set up, including customized Aerosol Jet Printed carbon-based sensors.

Results: The trends of RI observed at three different frequencies were able to describe cell growth and differentiation. In order to evaluate which frequencies better correlate with cell differentiation, Principal Component Analysis have been employed and the concordance analysis between RI magnitude and morphological, biochemical and molecular data, highlighted 40 kHz as the optimal frequency to assess Caco-2 cells differentiation process.

Conclusion: We demonstrated the feasibility and reliability of applying impedance-based measurements not only to provide information about the monolayer status, but also for cell differentiation monitoring.

General significance: This study underlined the possibility to use a dedicated sensor to assess the integrity and differentiation of Caco-2 monolayer, as a reliable non-destructive alternative to conventional approaches.

1. Introduction

It has long been known that cell models are a useful tool for the scientific research community. Among many others, Caco-2 cell line - derived from a human colorectal adenocarcinoma - is being widely used as a model of the intestinal barrier for the study of mechanisms underlying cancer development [1], toxicology [2] and, above all, for the analysis of absorption and metabolism processes in food science, nutrition [3] and drug discovery [4]. Indeed, Caco-2 cell line has been proposed as a model to investigate absorption mechanism at intestinal level, and many efforts have been performed to improve and standardize this line as a suitable alternative to more expensive and complex models such as the in vivo ones [5,6]. While deriving from colorectal cells, one of the best advantages in using this line is its ability to spontaneously differentiate into a monolayer when placed in culture, expressing several morphological and biochemical characteristics typically showed by mature small intestinal enterocytes [7,8]. Numerous studies revealed that differentiated Caco-2 cells grow in 21 days in a polarized monolayer characterized by domes, with microvilli on the apical side and tight junctions between adjacent cells. Furthermore they

Abbreviation: AJP, aerosol jet printing; ALPI, intestinal alkaline phosphatase; C_{Cell}, cell membrane/intercellular capacitance; CLDN4, claudin-4; CYP3A4, cytochrome P450 intestinal isoform; PCA, Principal Component Analysis; p-NP, p-Nitrophenol; p-NPP, *p*-Nitrophenyl phosphate; R_{Cell}, cell membrane/intercellular resistance; RI, relative impedance magnitude; rtPCR, real-time polymerase chain reaction; SI, sucrase-isomaltase; SLC11A2, solute carrier family 11 member 2; SLC15A1, solute carrier family 15 member 1; TEER, transendothelial electrical resistance; Z, impedance

* Corresponding author at: Department of Molecular and Translational Medicine, University of Brescia, Brescia, Italy.
E-mail address: m.marziano@unibs.it (M. Marziano).

https://doi.org/10.1016/j.bbagen.2019.02.008
Received 31 October 2018; Received in revised form 28 January 2019; Accepted 14 February 2019
Available online 25 February 2019
0304-4165/

express enzymes typical of mature enterocyte (i.e. alkaline phosphatase, sucrase-isomaltase, cytochrome P450) and definite intestinal transporters for sugar, oligopeptides, amino acids, vitamins and micronutrients [6,7]. Since the presence of an intact and differentiated barrier is crucial for in vitro experiments, non-invasive and non-destructive techniques are discovered, thus to easily quantify the barrier integrity and differentiation. Therefore, one of the mandatory objective required by the scientific community is the development of a methodology able to monitor the monolayer integrity and assess the differentiation of Caco-2 cells, in an easy, non-invasive and non-destructive way.

In this perspective, electrochemical sensors - able to detect specific variations in current, potential, capacitance, conductivity and, primarily, impedance signals - have been already demonstrated to be a non-invasive reliable method capable to provide useful and accurate information, concerning not only on cell adhesion [9], but also cell growth [10] and differentiation [11] processes.

In particular, impedance-based sensors - used as convenient and highly customizable technology - can provide real-time quantitative feedback on physiological processes [12,13]. In general, this technique requires the application of an alternating field voltage - with a constant amplitude (usually between 5 and 10 mV) and a defined range of frequency - to the measuring electrodes, and the measurement of the resulting alternating current. The overall impedance (Z) can be thence determined by applying Ohm's law [14,15]. Without cells the current flows freely from the surface to the electrodes; conversely, cells adherent on the electrode act as an insulator and impede the current flow, thus increasing the overall impedance of the system. More specifically, when cells are seeded on the substrate, they are almost spherical and the area of contact between basal membrane and the substrate surface is small, but it increases continuously while the cells spread. The cell membrane is essentially insulating and restricts current flow, depending also from its characteristic frequency. This non-invasive method can be applied to living cells and allows them to be monitored during growth and differentiation, since their morphological changes can be described by variations in impedance measurements [16]. Impedance-based cell monitoring appears as a promising tool not only for Caco-2 cells, but also for any other cell types. Furthermore, even if the technique was originally designed for two-dimensional applications, in the last decades, a huge interest has been addressed to translate it to three-dimensional sensing, thus to obtain information from cells directly embedded in 3D scaffolds [17,18]. In this picture, the use of conductive biomaterials [19,20] or of metallic external electrodes, both monopolar [21] or interdigitated [22] has been exploited in several literature works to perform impedance based cell monitoring of 3D cell cultures, with specific emphasis on the optimization of spatial sensitivity [23].

Considering the described approach and focusing on Caco-2 cells, we hypothesized that both the integrity of the monolayer and the cell differentiation could be monitored by evaluating the corresponding changes in the overall impedance [13,24]. Thus, the resulting value of overall impedance could give information concerning the capacitance of the cell layer, which can be related to cell differentiation, in addition to the trans-endothelial electrical resistance (TEER) – a parameter used to evaluate the integrity of the monolayer [25–27].

In this perspective, the aim of this work was to perform impedance measurements to specifically monitor growth and differentiation of Caco-2 cells by using dedicated sensors. More in detail, carbon-based interdigitated electrodes were outlined on polyimide substrate by means of an innovative Aerosol Jet Printing (AJP) methodology. Final sensors were seeded with cells, and impedance measurements were performed at different time intervals during the differentiation process (1–3–7-10-14-17-21 days after seeding). In addition, the relevance of such measurements in monitoring Caco-2 differentiation to enterocytes-like cells was evaluated comparing impedance measurements at different frequencies with the morphological, biochemical and molecular data.

2. Materials and methods

2.1. Cell culture

Commercial Caco-2 cell line (Sigma Aldrich,Merck KGaA) were routinely cultured in 100 mm dishes at 37 °C in humidified 5% CO_2 atmosphere. Dulbecco modified Eagle's medium was supplemented with 10% heat-inactivated fetal bovine serum, 2 mM glutamine, 50 μg/ml penicillin and 100 μg/ml streptomycin. For the differentiation experiments, cells were seeded at a density of 6×10^4 cells/cm^2 [28], cultured at 80% of confluence density and maintained for 21 days in complete medium, changing the medium three times a week [29]. All cell culture reagents were acquired from Sigma-Aldrich, Merck KGaA, Darmstadt, Germany.

2.2. Morphological assessment

In order to have a first feedback of the status of cell differentiation, initial morphological differences at different passages were evaluated by simply observing cell morphology changes with the microscope (Olympus, Italy) and counting domes, a characteristic feature used to evaluate Caco-2 to enterocyte-like differentiation [30]. Furthermore, the number and the dimension of domes evaluated with Fiji software (ImageJ Software).

2.3. Real-time PCR

Real-time PCR (rtPCR) was performed to quantify the expression of the following gene: sucrase-isomaltase (SI), intestinal alkaline phosphatase (ALPI), cytochrome P450 intestinal isoform (CYP3A4), claudin-4 (CLDN4), solute carrier family 15 member 1 (SLC15A1) and solute carrier family 11 member 2 (SLC11A2). After different days of differentiation (1–3–7-10-14-17-21), cells were harvested through trypsinization and the pellets were kept at −20 °C until RNA extraction. RNA was extract using TRIzol, chloroform and isopropanol (Sigma-Aldrich, Merck KGaA, Darmstadt, Germany). RNA (2 μg) was retro-transcribed using M-MLV reverse transcriptase (Promega, Madison, Wisconsin, USA), using random hexamers and the cDNA was then subjected to real-time PCR analysis with ViiA 7 Real-time PCR system (Applied Biosystems), using the iTaq™ Universal SYBR® Green Supermix (BIO-RAD, USA). The following specific primers (6 pmol) were used:

SI (s: AATCCTTTTGGCATCCAGATT, as: GCAGCCAAGAATCCCA AAT),
ALPI (s: CATACCTGGCTCTGTCCAAGA, as: GTCTGGAAGTTGGCCT TGAC),
CYP3A4 (s: GATGGCTCTCATCCCAGACTT, as: AGTCCATGTGAAT GGGTTCC),
CLDN4 (s: TCCGCCAAGTATTCTGCTG, as: CGTGGCACCTTACACG TAGTT),
SLC15A1 (s: TCTCTGTCACGGGATTGGA, as: CTGCCTGAAGCACCG ACT),
SLC11A2 (s: CACCGTCAGTATCCCAAGGT, as: CCGATGATAGCCAA CTCCAC),
TBP (s: GAACATCATGGATCAGAACAACA, as: ATAGGGATTCCGGG AGTCAT).

The PCR program was initiated by 10 min at 95 °C before 40 cycles, each one of 1 s at 95 °C and 30 s at 60 °C. Experiments were done in biological and technical triplicate and expression data were normalized using the Ct of the internal control TBP [29,31].

2.4. Alkaline phosphatase assay

ALPI activity was assayed using the substrate *p*-Nitrophenyl phosphate (p-NPP) and evaluating the yellow product p-Nitrophenol (p-NP)

formation (Sigma-Aldrich, Merck KGaA, Darmstadt, Germany) detected spectrophotometrically at 405 nm. ALPI was measured during differentiation (1-3-7-14-17-21 days after seeding), by applying a standardized method on cell homogenates adapted from [32]. Briefly, after washing the cells at 4 °C with PBS with 1 mM $CaCl_2$ and 1 mM $MgCl_2$, Caco-2 cells were harvested with scraper into 500 µl of ALPI collection buffer (10 mM Tris-HCl, 150 mM NaCl ph 8.0) on ice. Then, cells were sonicated 5 times for 5 s, quantified with Bradford's method (BIO-RAD, USA) and kept at −20 °C until the enzymatic assay. The activity was measured transferring cell homogenate in pNPP solution (2.5 mg/ml pNPP dissolved in Tris 0.2 M pH 9.5) in a reaction tube and then incubating at 37 °C. At various time intervals (2–4–6-8 min) 100 µl of reaction were transferred from the reaction tube to the 96-well plate containing 25 µl of 0.5 M NaOH. Enzyme activity was calculated by means of a standard curve prepared with different concentration of pNP (0–50–100-200-300-400-500-600 µM). Data were expressed as µg of pNP normalized over the amount of µg of total protein and experiments have been performed in triplicate.

2.5. Sensors production

For the production of the sensors, Kapton® MT polyimide film with a thickness of 25 µm was purchased from DuPont (USA) whereas an electrically conductive carbon-based ink (EXP 2652–28, sheet resistivity 100 Ω/sq./mil) was acquired from Creative Materials (USA). Since the final aim of this work was to monitor the adhesion, growth and differentiation of a large population of cells, an interdigitated geometry was designed by a commercial CAD (AutoCAD 2017) [33], taking into account the necessity to realize a sensor compatible with 24 multiwells plates for cell cultures. The defined electrodes geometry was printed with the carbon-based ink by an AJP (AJ printer 300-UP, Optomec, USA). This technique works with liquid suspensions which are nebulized thanks to a carrier gas, and then focused on the substrate realizing features in the range of 100 nm-10 µm in thickness and 10 µm to 5 mm for line width. The developed sensors have a diameter of 13 mm including 2 interdigitated electrodes (Fig. 2A). In order to fit the plate, printed polyimide substrate was cut into circles (diameter 14 mm) with a mechanical puncher. Particular care was put in the design and printing of the interdigitated electrodes thus to obtain tracks 50 µm wide, thanks to the lateral resolution ensured by the AJP (around 10 µm). This level of accuracy of the printing process ensured to reach dimensions of each electrode fingers in the order of magnitude of cells (around 10 µm). Thus, the number of cells sensed by each finger could be reduced and the overall sensitivity to evaluate their number and reciprocal position increased, in comparison with screen printed or inkjet-printed sensors, where best resolution is around 50–100 µm. In order to reduce the overall resistance of each interdigitated electrodes (< 1 kΩ), two subsequent layers of carbon-based ink were deposited. After the deposition, sensors were cured for 15 min at 150 °C. The sensors were then sterilized and fixed to the bottom of wells with a biocompatible high vacuum grease that prevented their floating in the culture medium.

2.6. Impedance measurements

Impedance measurements in term of magnitude and phase angle were carried out by considering a standardized protocol and using a commercial portable potentiostat (Palmsens PS Trace, PalmSens BV, Netherlands) applying a sinusoidal voltage to the sample and measuring the current response in the range of frequencies from 400 Hz and 50 kHz. Measurements were performed before and after cell seeding, in order to correlate variations in the electrical properties with cell adhesion, growth and differentiation. All the pre-seeding tests were carried out with the medium after performing poly-L-lysine (Sigma-Aldrich, Merck KGaA, Darmstadt, Germany) coating, thus to obtain a value of reference, to be compared with after-seeding measurements. The measurements realized after cell seeding (6×10^4 cells/cm^2) were performed at different time points (1–3–7-10-14-17-21 days after seeding), in order to follow the variation of impedance characteristic spectra (i.e. impedance magnitude and phase angle with respect to frequency) during the differentiation process. Experiments were performed in quadruplicate. Data were analyzed by evaluating the impedance magnitude at low, medium and high frequencies (400 Hz, 4 kHz and 40 kHz), in order to assess the most sensitive ones for cells growth and differentiation monitoring. Results have been then expressed as relative impedance magnitude (RI), calculated as $RI = ((|Z|_{\text{with cells}} - |Z|_{\text{without cells}}))/|Z|_{\text{without cells}} * 100)$ [34].

2.7. Equivalent circuit modeling

For further analysis of impedance spectra alterations, phase angle and magnitude spectra were fitted on an electronic equivalent circuit model, used to describe tissue-electrode interface [15,35]. Parameters of the equivalent circuit were determined by means of a two-step optimization procedure considering the measurements performed by sweeping all the frequencies from 400 Hz to 50 kHz. First, the contribute of the not-seeded sensors was modeled considering a reduced equivalent circuit, i.e. including electrodes and solution electrical contributes (resistance R_{Cell}, capacitance C_{Cell} of the electrode, and resistance R_{medium} of the solution), but without considering the cell-specific contribution. Subsequently, the cell-covered electrodes were analyzed by applying the entire equivalent circuit, thus including cell membrane/intercellular capacitance (C_{Cell}) and resistance (R_{Cell}), including both the contributes of cell membrane and of the extracellular resistance, determined by the fitting procedure. The fitting procedure and the corresponding analysis was performed with PS Palmsens Trace dedicated software.

2.8. Statistical analysis

Statistical analyses were performed using Graph Pad Prism version 5.0 (Graph Pad Software Inc., San Diego, CA, USA). All values are presented as mean ± standard error of mean (SEM) unless otherwise designated. Statistical significance of differences was determined by one-way ANOVA, followed by the Bonferroni test. Student's *t*-test was also used to compare values in different groups.

Further, in order to extract a component score which is a linear combination of the different impedance measured at three selected frequencies, the Principal Component Analysis (PCA) [36] was also included. In addition, correlation coefficients of multiple method data progression were determined applying two-tailed Pearson correlation test ($\rho > |0.7|$) and the statistical significance is considered when p-value < .05 [13]. The concordance between two measure was also analyzed by using the Bland-Altman plots [37,38], after standardizing the data (means = 0; variance = 1) in order to solve scale problem related to measures extremely different in magnitude. In details, it displays the mean (x-axis) and the differences (y-axis) of the two measures in a scatterplot. The 95% of confidence interval (red line) is computed around the grand mean of the differences (green line). Two measures are concordant when dots are randomly distributed around the grand mean. PCA, Person test and Bland-Altman plot were performed by using R version 3.5.1.

3. Results and discussion

3.1. Morphological, biological and biochemical characterization of cell differentiation

Cells seeded at a density of 6×10^4 cells/cm^2 reached the confluence after few days from the seeding and started to create domes at the seventh day after seeding (Fig. 1A) and both domes number and area increased with the increasing days of differentiation (Fig. 1B).

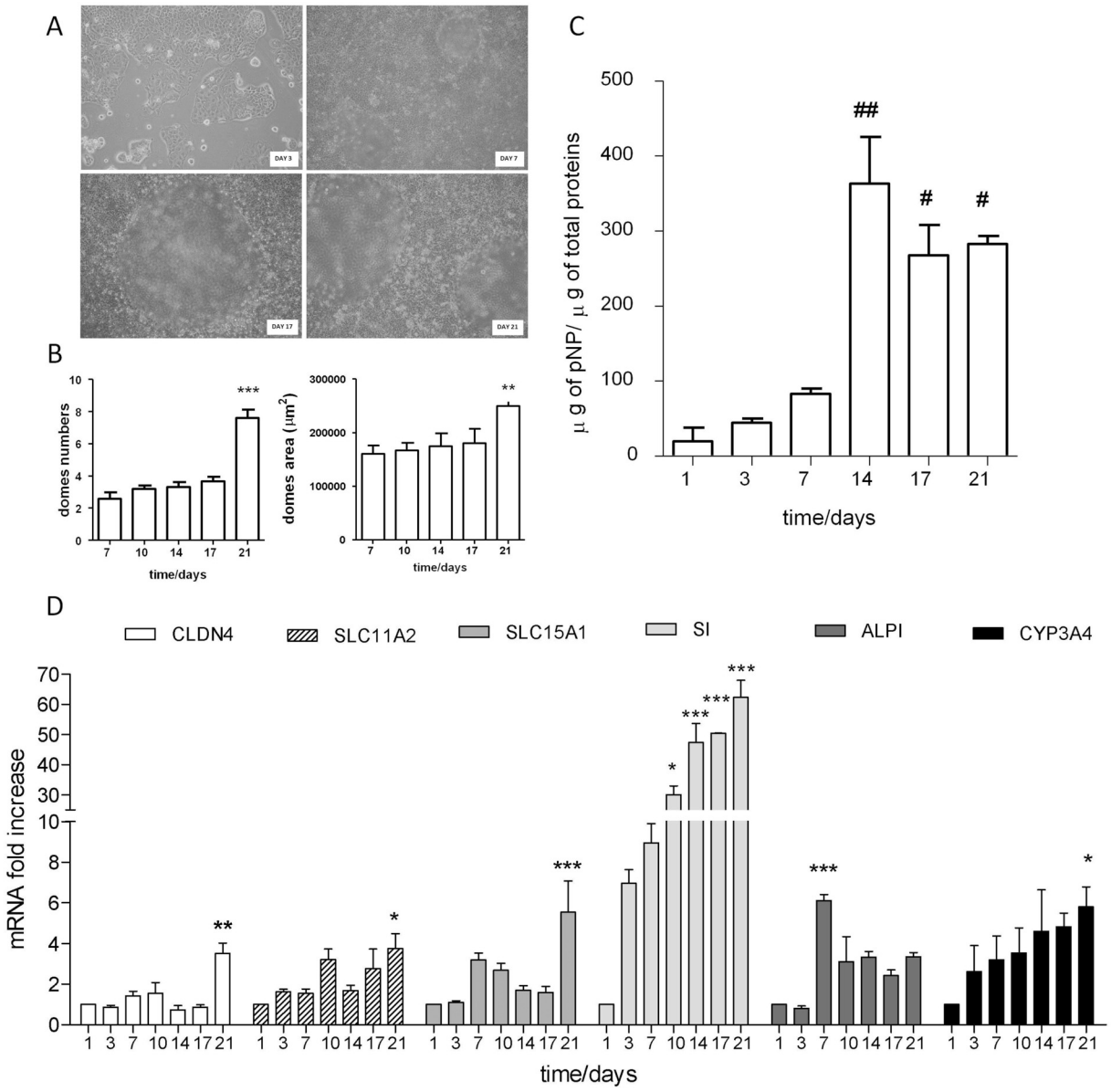

Fig. 1. Caco-2 cells undergo intense morphological and physiological changes during spontaneous enterocyte-like cells differentiation. A) Representative pictures of Caco-2 cells morphological evaluation at four different time-points (days 3-7-17-21) during 21 days differentiation protocol (magnification 4× in day 3 and 7; magnification 10× in day 17 and 21); B) Domes counting and measuring. The statistical significance was represented as follows:**p < .01; ***p < .001 versus the seventh day after seeding (no domes formation before day 7); C) ALPI assay. μg of pNP extrapolated by a standard curve at days 1-3-7-14-17 and 21 after seeding. Data are normalized for total protein amount (#p < .05, ##p < .01 versus the corresponding day 1 as control group); D) Quantitative rt-PCR time-courses of key genes CLDN4, SLC11A2, SLC15A1, SI, ALPI, and CYP3A4 during 21 days of differentiation. The values are expressed as mRNA fold increase compared to day 1 for each genes. The statistical significance was *p < .05; **p < .01; ***p < .001 versus the corresponding day 1 of each gene as control group.

To further evaluate Caco2-cells spontaneously differentiated into mature enterocytes, we followed the mRNA expression levels of some intestinal markers during the 21 days of differentiation. In particular, we specifically evaluated some small intestinal enzymes such as SI, ALPI and CYP3A4. In addition, we evaluated the gene expression of CLDN4 which encodes an integral membrane protein that is component of the epithelial cell tight junctions. Finally, for brush border transporters, we analyzed SLC15A1 which encodes an intestinal hydrogen peptide cotransporter protein that plays an important role in the uptake and digestion of dietary proteins and SLC11A2 that encodes a member of the solute carrier family 11 protein family involved in the transport of divalent metals and in iron absorption. SI and CYP3A4 showed a progressive increase during differentiation that became statistically significant starting from day 10 for SI and from day 17 for CYP3A4 (Fig. 1D). SI is commonly expressed in the adult small intestine where, as a brush border hydrolase, it is involved in the final steps of digestion of sucrose, starch and glycogen. Its expression is limited to the villous enterocyte. CYP3A4 the principle cytochrome P450 present in human liver and small intestinal epithelial cells (enterocytes) has been implicated in several transport functions, including the transport of some drugs [39]. Together with the intestinal alkaline phosphatase, it is often used as a marker of terminal differentiation of enterocytes [31,40]. In our experiments, ALPI mRNA expression substantially showed a peak when the domes appeared at day 7. From day 10, its expression decreased but remained anyway higher if compared with the day 1 and 3, when the culture was not yet at confluence. This trend for ALPI is confirmed also by other authors [31,32]. RNA expression of CLDN4, significantly enhanced at day 21 after seeding. Similarly, the two genes SLC15A1 and SLC11A2, whose encoded products, are members of solute carrier families, showed higher mRNA expression when enterocytes

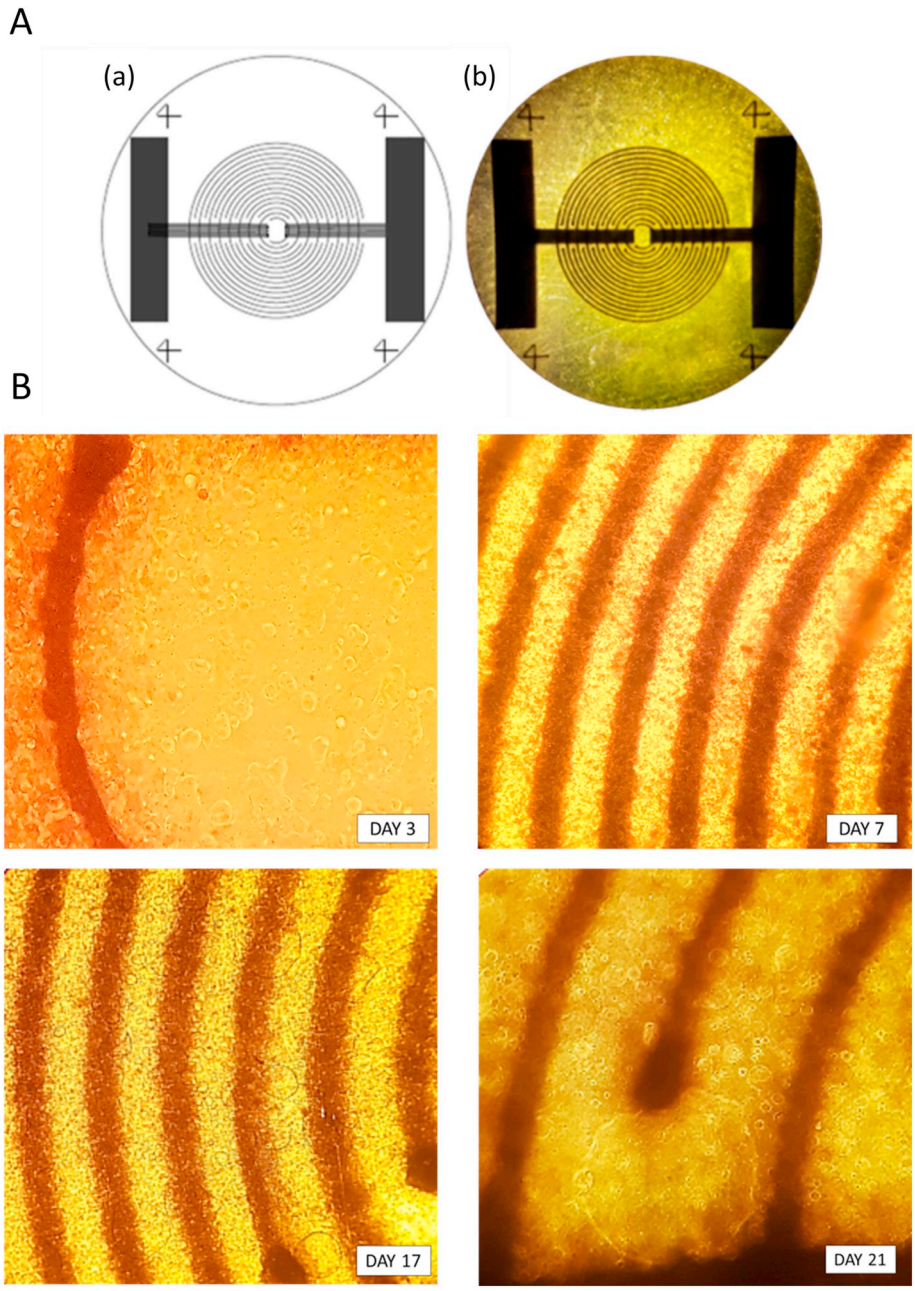

Fig. 2. Caco-2 to enterocyte-like cells differentiation on interdigitated carbon-based electrodes printed on a polyimide substrate. A) Printed Sensor geometry optimized with AutoCAD 2017 (a) and image of the sensor acquired with microscope (magnification 1×) (b). B) Representative pictures of Caco-2 cells evaluation at four different time-points (days 3–7–17-21) during 21 days differentiation protocol (magnification 10× and 20× for day 21) where sensor geometry is clearly visible. The 21 day picture results out of focus to better visualize the domes.

are completely differentiated. These results confirmed not only the structural maturation (i.e. CLDN4) but also the functional differentiation with an increase of enzyme expression typical of mature enterocytes (SI, ALPI and CYP3A4), and small intestine transporters (SLC15A1 and SLC11A2). These data are consistent with results already reported in the literature [29,31].

In addition, data regarding the ALPI enzymatic activity in cell homogenates corroborated the effective complete functional differentiation of Caco-2 cells to enterocytes. In fact, ALPI enzymatic activity, measured as μg of pNP product over total protein, significant increased starting from day 14 (Fig. 1C). That ALPI activity linearly increases during differentiation of enterocytes is well recognized, and it is therefore considered another marker of Caco-2 cell differentiation in vitro [41]. All this information initially confirmed the proper occurrence of the differentiation process.

3.2. Impedance measurements during Caco-2 cell differentiation

One of the main hurdles regarding Caco-2 cell enterocyte-like differentiation is the lack of non-invasive and non-destructive method for quantitatively monitoring the integrity of the monolayer and assess the differentiation process. Common biological and biochemical methods such as rtPCR and enzymatic assays are in fact expensive, invasive and destructive. To overcome these limits, we investigated the possibility to apply the electrical impedance analysis to monitor the differentiation process and verify the monolayer integrity. In order to achieve this goal, an impedance-based measurement setup was designed and realized, including dedicated sensors, specifically customized and realized

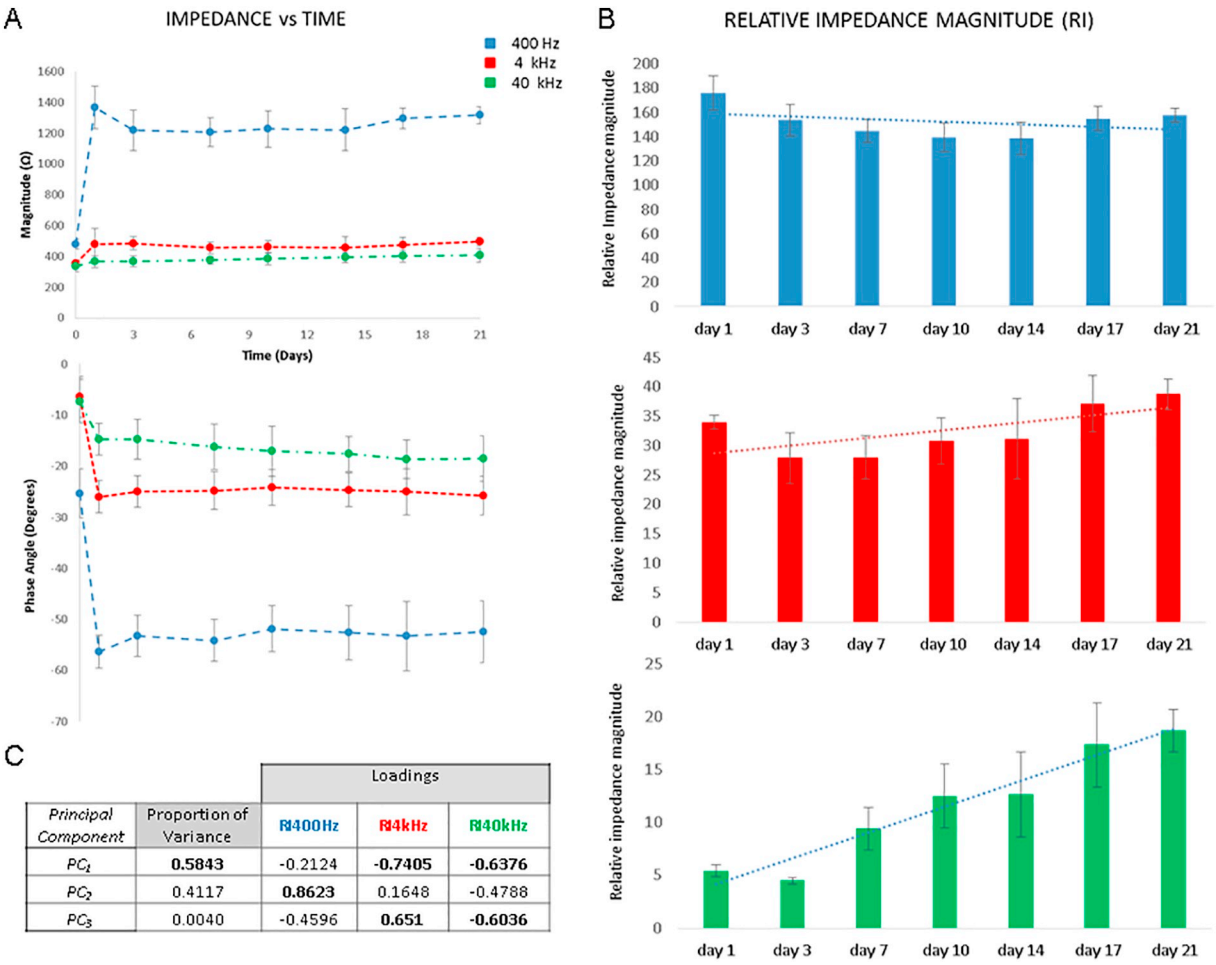

C

Principal Component	Proportion of Variance	Loadings RI400Hz	RI4kHz	RI40kHz
PC_1	**0.5843**	-0.2124	**-0.7405**	**-0.6376**
PC_2	0.4117	**0.8623**	0.1648	-0.4788
PC_3	0.0040	-0.4596	**0.651**	**-0.6036**

Fig. 3. Impedance-based cell monitoring vs time and relative impedance calculation. A) Impedance magnitude vs time during the differentiation process. Error bars show the standard deviation of the 5 sensors evaluated. B) Variation of the relative impedance during the 21 days of cell culture, calculated for each of the frequencies evaluated: low (400 Hz-blue) medium (4 kHz-red) and high (40 kHz-green). C) Principal component analysis. The proportion of variance (0.5843) could be represented as a percentage (about 60%) and PC_1 is the first component with the largest possible variance explained; succeeding components (PC_2 and PC_3) are orthogonal to PC_1 with the highest possible variance.

by means of AJP (Supplementary Fig. 1). First, the choice of carbon-ink and polyimide substrate was specifically performed after a deep analysis, assessment and comparison of several inks and materials [42], taking into account the necessity to realize a sensor cytocompatible and resistant to common sterilization processes (e.g. autoclave). The interdigitated geometry of the sensors was demonstrated to be more suitable for cell population monitoring, if compared to the monopolar one [43,44]. Indeed, this specific configuration has been gaining more and more popularity and it is extensively used for different application in biological sensing [45,46]. Here, we designed circular interdigitated sensors of 14 mm diameter that fitted with 24 multi-well plate (Fig. 2A). When cells were seeded on the biosensors and cultured for 21 days, they grew well and differentiated at a mature enterocyte monolayer, as showed by the characteristic dome formation (Fig. 2B). This results were in line with data reported in literature on the biocompatibility of the interdigitated carbon ink printed on polyimide substrate [42]. The production by means of printed flexible electronics represents a real promising tool able to combine cost and time effectiveness, with the maximum possibility of customization and optimal geometric and electronic performances. It ensures the possibility to easily tune the electrical resistance of the electrodes, by changing the number of printed layers and the duration of the curing, but also the geometrical parameters of the sensor, by tuning ink viscosity, and printer parameter [47]. Furthermore, compared with more traditional printing techniques such as ink jet or screen printing, AJP allows to achieve resolution in the order of 10 μm with a very high repeatability, features that are particularly valuable for application in biological assays [48].

Comparing the impedance magnitude and phase angle variation after cell seeding at different frequencies, a significant initial increase of the impedance magnitude, with the maximum value of 1 kΩ recorded at low frequency (400 Hz) and a decrease of the phase angle toward a capacitive-like behavior [49,50], with the maximum decrease recorded at lower frequencies (−30 degrees), could be observed suggesting an effective cell adhesion (Fig. 3A). This suggests that the seeded cells effectively adhered on the sensors acting as an insulating layer on the electrodes, forcing the low frequency current to flow around the cellular bodies on paracellular pathways, thus strongly increasing the ohmic resistance of the total system compared with the pre-seeding condition. The decrease in impedance recorded at 400 Hz and 40 kHz during day 3 can be presumably due to cells crowd resulting in more regions of cell-cell contact and a slight drop in resistance. This factor appears to be essentially highly reduced at high frequencies, in agreement with the literature [51,52]. Thus, at low frequencies the majority of the current tends to flow below or in between cells while at high frequencies the current goes through the cells. Consequently, the high frequency impedance, more affected by cell-coverage, is more influenced from the formation of domes, whereas the low frequency, responding more strongly to changes in the spaces either under or between the cells, better follows the adhesion process at day 1 and the tight junction formation at day 21. Fig. 3B reported the relative

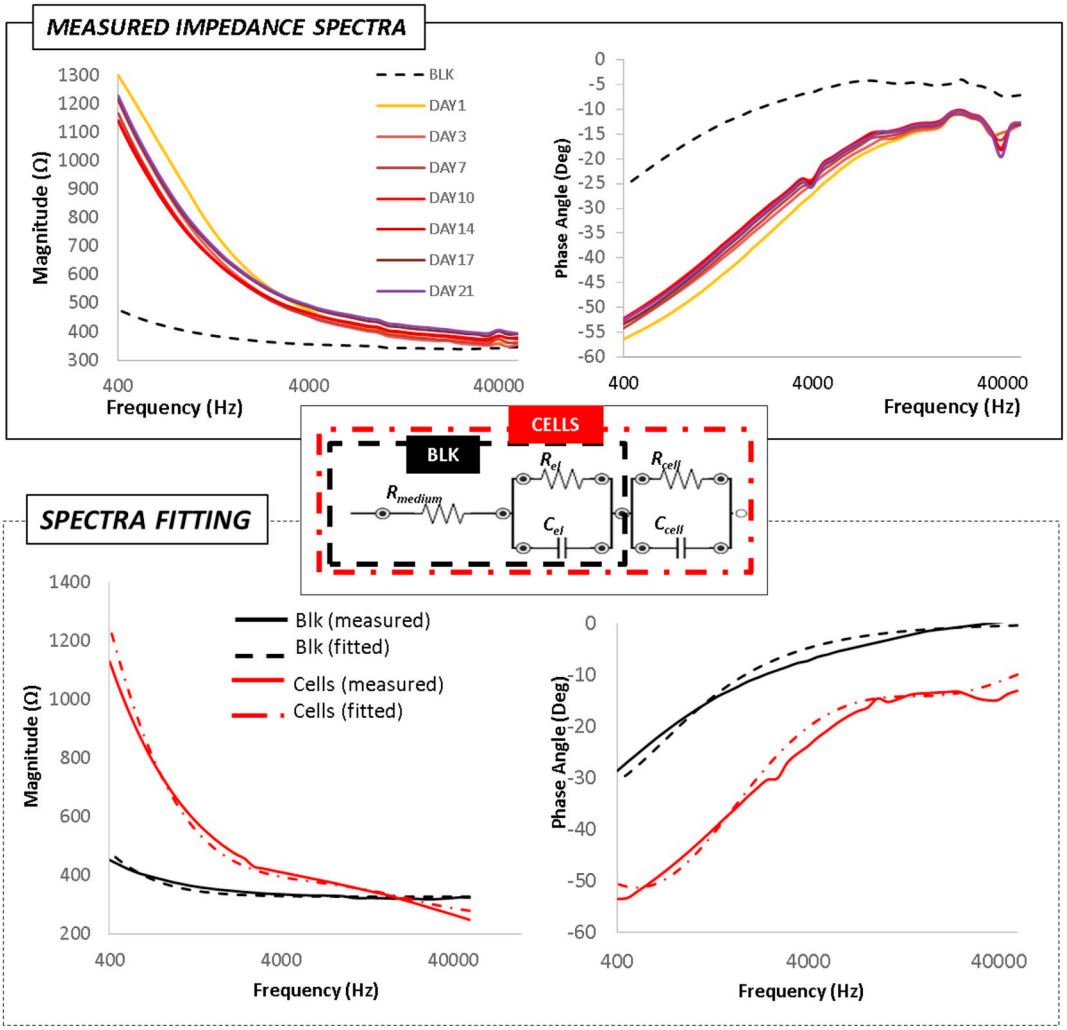

Fig. 4. Impedance-based cell monitoring vs frequency and spectra fitting with equivalent circuit: a) Impedance magnitude and phase spectra vs frequency during the differentiation process. b) Equivalent circuit of blank and seeded sensors used to fit the spectra.

impedance magnitude (RI), normalized over the background, at the three different frequencies, 400 Hz, 4 kHz and 40 kHz. Interestingly, a significant increase of RI during the 21 culturing days was observed at 40 kHz, and a similar but weaker trend was found at 4 kHz, suggesting that the monitoring of RI at these two frequencies might be useful to follow the Caco-2 cell growth and differentiation.

More in detail, the trend of RI observed at these frequencies allowed to recognize three interesting moments of cell growth and differentiation (Fig. 3). As previously discussed, the first increase observed at day 1, maximum at low frequencies, could be correlated with the initial capacitive coupling of the current directly through the insulating cell membranes of the initially attached cells. After that, the following monotone increase recorded between day 3 and day 10 can be associated with cells growth on the sensors. Due to cell proliferation and spreading, the percentage of sensor's surface covered by cells increases and the current has to flow through them, affecting the overall measured impedance. Finally, the increase recorded between day 15 and day 21, concluding with a sort of plateau suggesting the effective formation of a confluent and tight layer of cells, supporting our hypothesis of correlation with cell differentiation.

At this regards, to better evaluate which frequencies could better highlight Caco-2 to enterocytes-like cells differentiation we combine the multiple measures of impedance by using the Principal Component Analysis (PCA), an exploratory statistical method that converts a set of observations of possibly correlated variables into a set of values linearly uncorrelated called Principal Components (PCs). Thus, it is possible to extract the loadings that represents the weight of each standardized variable (RI at 400 Hz, 40 kHz and 4 kHz) within the PC_1 component score. In details, as reported in Fig. 3C, the first component PC_1, where RI 4 kHz and RI 40 kHz have a greater weight, was able to describe nearly the 60% of explained variance.

All these data are supported from literature, since the specific frequencies 40 kHz and 4 kHz have been previously highlighted as two of the most sensitive for recognizing cells coverage during electric impedance measurements [53]. In particular, the highest sensitivity that can be observed at 40 kHz from the trendline of the RI during the 21 days, appears to be coherent with findings observed by Wegener et al. [16], where this specific frequency has been indicated as the most sensitive ones for monitoring Caco-2 cells using an impedance based technique.

Respect to widely used TEER where a pair of chopstick electrodes are used to measure the resistance between the apical and the basolateral compartment [54], our impedance-based sensors represent a different approach, less expensive and with a more uniform and coherent monitoring of the impedance both in terms of magnitude and phase angle, with a complete analysis over a range of defined frequencies.

3.3. Equivalent circuit modeling

Electric circuit model of adherent cells on conductive electrodes has

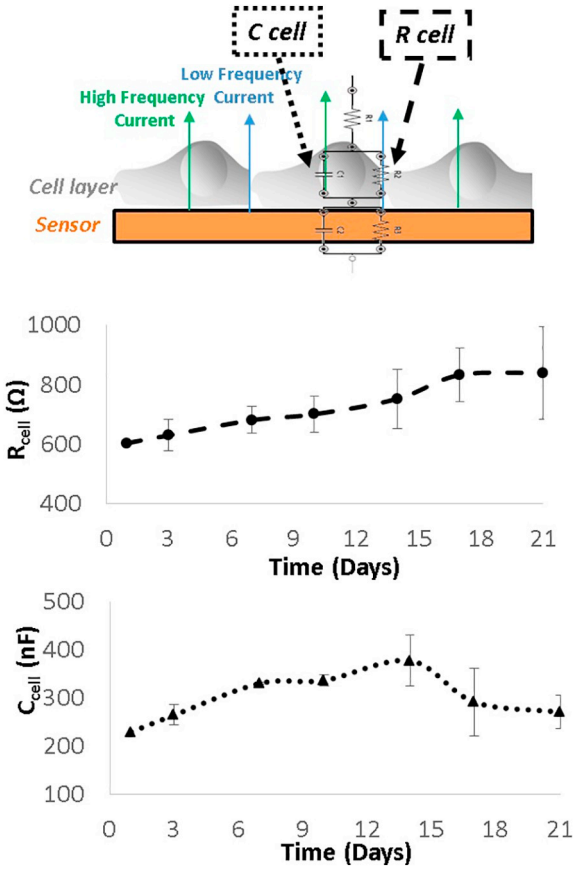

Fig. 5. Evolution of R_{cell} and C_{cell} during differentiation: above, schematic of correspondence between the different parameters in the model with the circuit element; below, specific evolution of the modeling circuit parameters related to cells attached on the sensors.

A

	RI4kHz	*RI40kHz*	*p-value* (RI 40kHz)
RI4kHz	1		
RI40kHz	0.7255	1	
CLDN4	0.4969	0.5577	0.1933
SLC11A2	0.5410	**0.8199**	***0.0239***
SLC15A1	0.3680	0.6318	0.1279
SI	0.6902	**0.9427**	***0.0015***
ALPI	-0.1764	0.3556	0.4338
CYP3A4	0.5081	**0.9134**	***0.0040***
Domes numbers	0.8038	0.7933	0.1093
Domes area	0.8137	0.8008	0.1035
ALPI enzyme activity	0.4898	**0.8300**	***0.0409***

B

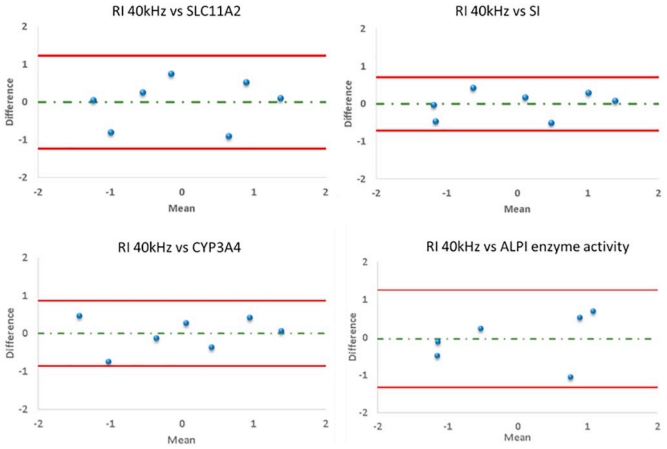

Fig. 6. A) Pearson correlation coefficients table. Significant correlations is considered for $\rho > |0.7|$ (grey) and the statistical significance is obtained with correlation test and reported in bold (p-value reported for RI at 40 kHz is accepted when < 0.05); B) Bland-Altman plots represent the differences between the pairs of readings, visualizing the pattern of agreement of statistically significant measurements (RI at 40 kHz vs SLC11A2, SI, CYP3A4 and ALPI enzyme activity). Data are standardized (means = 0; variance = 1) to solve scale problem. The 95% of confidence interval (red line) is computed around the grand mean of the differences (green line).

been widely investigated by several groups, including different levels of circuit complexity depending on the specific features that the impedance-based measurement aimed to highlight.

Literature reports models ranging from the simplest circuit – which considers just the overall resistive and capacitive contribute of cells [55] to the more complex ones which analyze the contribute of each specific cell components (attached membrane and superior membrane, cytoplasm, organelles and protein across the membrane) [50]. In our model we choose a specific circuit including only the components required to model the predominant behavior of all the elements involved (cells, electrodes and medium). More in detail, the electrolytic solution was modeled as a constant resistance (R_{medium}), the electrodes as a parallel RC (R_{Cell} and C_{Cell}) and cell coverage as well as an additional parallel RC (R_{cell} and C_{cell}). While R_{Cell}, C_{Cell} and R_{medium} could be considered constant in all the fitting, R_{cell} provided useful information about the effective adhesion of the cells, on their proximity and on the tight junction presence. C_{cell} instead, more sensitive to the number of the cells and on the multiple layers, provided a feedback on the increase of cell number and on domes formation. Using the described circuit, the impedance spectra obtained from measurements without and with cells seeded on the sensor at the different timepoints (Fig. 4A) could be analyzed with the circuit described above, as presented in Fig. 4B, where measured and fitted spectra are graphed together in order to better highlight the approximation performed with the circuit considered.

The analysis performed with the modeling approach is able to provide us with information on the gap left between the cells and to highlight the contribution of adhering cells on the electrode surface. Both the resistive and the capacitive components can be integrated in the circuit and compared to the cell-free model (Fig. 5). Regarding R_{cell}, the highest increase (around 600 Ω) could be measured during the first 24 h, due to the reduction of the paracellular pathways available for low frequency current paths, suggesting an effective adhesion of cells. After the first day, the resistance kept on increasing, until day 21, showing a plateau after the day 17, suggesting a complete differentiation of the monolayer. Regarding C_{cell}, it increases during the first 15 days of differentiation, due to the double layer capacitive contribute of the cell membranes on the electrodes. Then, after a maximum reached around day 15, it decreases in the last two time points. Results obtained both for R_{cell} and for C_{cell} appear in agreement with what found by using different cell types. In detail, as referred also in [54,56], where endothelial cells were involved, the R_{cell} appears to show a high increase due to the adhesion and then a slow increase due to proliferation, with a sort of plateau corresponding to the monolayer formation. Differently, C_{cell} evolution can be correlated with the number of cells and in particular with their morphological changes due to differentiation process. It appears to increase until confluence is reached and then is reduced when domes, the typical structure of enterocyte-like cells, are created. This decrease in the overall capacitance can be explained taking into consideration the domes structure, which can be modeled as a series of capacitors [57]. In addition to the pure impedance analysis, the proposed modeling approach allowed to analyze both resistance and capacitance giving additional information about the

barrier properties and cell processes such as adhesion, growth and differentiation [49].

3.4. Concordance between relative impedance magnitude and morphological, biochemical and molecular data

In order to highlight possible concordance between changes in impedance magnitude and other parameters related to cell differentiation, a Pearson correlation analysis was performed, specifically considering RI at the two frequencies (4 kHz and 40 kHz) and the PC_1 obtained excluding 400 Hz. In fact, the re-computed PC_1 described nearly the 86% of explained variance and the two frequencies (40 kHz and 4 kHz) had the same weight (−0.7071). In particular, the Pearson analysis reported in Table in Fig. 6A, described the linear relationship between the behavior of RI with that of the biological, morphological and biochemical parameters during the differentiation process. Interestingly to note, among different frequencies, RI measured at 40 kHz better correlate with the other variables. We specifically found a good statistically significant correlation during the 21 days of differentiation between the increase of RI at 40 kHz and SLC11A2 ($\rho = 0.8199$ and $p = .0239$); SI ($\rho = 0.9427$ and $p = .0015$), and CYP3A4 ($\rho = 0.9134$ and $p = .0040$) genes mRNA expression (Table in Fig. 6A). On the contrary, no correlation was found for CLDN4, SLC15A1 and ALPI genes, despite for this latter a good correlation was at least found for its enzyme activity ($\rho = 0.8300$ and $p = .0409$). Although a good correlation between RI at 4 kHz and 40 kHz with morphology (domes numbers and area) was found, it was not statistically significant, probably due to the small sample size tested. Interestingly, when Pearson test is performed using PC_1 the correlation coefficients are reduced, confirming the relevance of 40 kHz respect to 4 kHz. (Supplementary Fig. 2). Moreover, the strong and significative correlation between RI 40 kHz and SLC11A2, SI, CYP3A4 and ALPI enzyme activity has been also confirmed by the Bland-Altman plots, where the dots (blue) are randomly distributed closely around the grand mean (green).

4. Conclusion

In conclusion, we reported the feasibility and reliability of an additional method for monitoring cell differentiation of Caco-2 to enterocyte-like cells, based on impedance measurements. Using AJP as powerful technique to achieve high resolution printed electronics, customized interdigitated sensors have been designed and realized depositing a carbon-based ink on flexible polyimide, obtaining low-cost sensors easy to sterilize and integrate with cell culture routine. Results derived from the statistical analysis, performed to evaluate the concordance between morphological, biochemical and molecular data and impedance outputs, allowed to highlight 40 kHz as the optimal frequency to assess Caco-2 to enterocyte-like cells differentiation process. Overall, these results support the here-presented non-invasive and non-destructive approach not only to assess the barrier integrity, but also for cell differentiation monitoring during in vitro experiments.

Author statement

Marziano M.: Conceptualization, Methodology, Validation, Formal Analysis, Investigation, Data Curation, Writing – Original Draft

Tonello S.: Methodology, Validation, Formal Analysis, Investigation, Data Curation, Writing – Original Draft

Cantù E.: Methodology, Writing – Review & Editing

Abate G.: Methodology, Formal Analysis, Data Curation, Writing – Review & Editing

Vezzoli M: Methodology, Formal Analysis, Data Curation, Writing – Review & Editing

Rungratanawanich W.: Methodology, Writing – Review & Editing

Serpelloni M.: Writing – Review & Editing

Lopomo N.F.: Writing – Review & Editing

Memo M.: Writing – Review & Editing

Sardini E.: Writing – Review & Editing, Funding Acquisition

Uberti D.: Conceptualization, Project Administration, Supervision, Writing – Review & Editing, Funding Acquisition

Appendix A. Supplementary data

Supplementary data to this article can be found online at https://doi.org/10.1016/j.bbagen.2019.02.008.

References

[1] A. Ferraretto, C. Gravaghi, E. Donetti, S. Cosentino, B.M. Donida, M. Bedoni, G. Lombardi, A. Fiorilli, G. Tettamanti, New methodological approach to induce a differentiation phenotype in Caco-2 cells prior to post-confluence stage, Anticancer Res. 27 (2007) 3919–3925.

[2] A. Garcia-Lorenzo, E. Tojo, J. Tojo, M. Teijeira, F.J. Rodriguez-Berrocal, M.P. Gonzalez, V.S. Martinez-Zorzano, Cytotoxicity of selected imidazolium-derived ionic liquids in the human Caco-2 cell line. Sub-structural toxicological interpretation through a QSAR study, Green Chem. 10 (2008) 508–516 https://doi.org/10.1039/B718860A.

[3] T. Langerholc, P.A. Maragkoudakis, J. Wollgast, L. Gradisnik, A. Cencic, Novel and established intestinal cell line models - an indispensable tool in food science and nutrition, Trends Food Sci. Technol. 22 (2011), https://doi.org/10.1016/j.tifs.2011.03.010.

[4] R.B. van Breemen, Y. Li, Caco-2 cell permeability assays to measure drug absorption, Expert Opin. Drug Metab. Toxicol. 1 (2005) 175–185, https://doi.org/10.1517/17425255.1.2.175.

[5] T. Lea, Caco-2 cell line, in: K. Verhoeckx, P. Cotter, I. López-Expósito, C. Kleiveland, T. Lea, A. Mackie, T. Requena, D. Swiatecka, H. Wichers (Eds.), Impact Food Bioact. Heal. Vitr. Ex Vivo Model, Springer International Publishing, Cham, 2015, pp. 103–111, , https://doi.org/10.1007/978-3-319-16104-4_10.

[6] Y. Sambuy, I. De Angelis, G. Ranaldi, M.L. Scarino, A. Stammati, F. Zucco, The Caco-2 cell line as a model of the intestinal barrier: influence of cell and culture-related factors on Caco-2 cell functional characteristics, Cell Biol. Toxicol. 21 (2005) 1–26, https://doi.org/10.1007/s10565-005-0085-6.

[7] I.J. Hidalgo, T.J. Raub, R.T. Borchardt, Characterization of the human colon carcinoma cell line (Caco-2) as a model system for intestinal epithelial permeability, Gastroenterology. 96 (2018) 736–749, https://doi.org/10.5555/uri:pii:0016508589908974.

[8] M.J. Engle, G.S. Goetz, D.H. Alpers, Caco-2 cells express a combination of colonocyte and enterocyte phenotypes, J. Cell. Physiol. 174 (1998) 362–369, https://doi.org/10.1002/(SICI)1097-4652(199803)174:3<362::AID-JCP10>3.0.CO;2-B.

[9] A. Kourtidis, S.P. Ngok, P. Pulimeno, R.W. Feathers, L.R. Carpio, T.R. Baker, J.M. Carr, I.K. Yan, S. Borges, E.A. Perez, P. Storz, J.A. Copland, T. Patel, E.A. Thompson, S. Citi, P.Z. Anastasiadis, Distinct E-cadherin-based complexes regulate cell behaviour through miRNA processing or Src and p120 catenin activity, Nat. Cell Biol. 17 (2015) 1145–1157, https://doi.org/10.1038/ncb3227.

[10] T.N. MacKenzie, N. Mujumdar, S. Banerjee, V. Sangwan, A. Sarver, S. Vickers, S. Subramanian, A.K. Saluja, Triptolide induces the expression of miR-142-3p: a negative regulator of heat shock protein 70 and pancreatic cancer cell proliferation, Mol. Cancer Ther. 12 (2013) 1266–1275, https://doi.org/10.1158/1535-7163.MCT-12-1231.

[11] J.I. Alvarez, A. Dodelet-Devillers, H. Kebir, I. Ifergan, P.J. Fabre, S. Terouz, M. Sabbagh, K. Wosik, L. Bourbonniere, M. Bernard, J. van Horssen, H.E. de Vries, F. Charron, A. Prat, The hedgehog pathway promotes blood-brain barrier integrity and CNS immune quiescence, Science 334 (2011) 1727–1731, https://doi.org/10.1126/science.1206936.

[12] I. Giaever, C.R. Keese, Use of electric fields to monitor the dynamical aspect of cell behavior in tissue culture, IEEE Trans. Biomed. Eng. 33 (1986) 242–247, https://doi.org/10.1109/TBME.1986.325896.

[13] D. Seidel, J. Obendorf, B. Englich, H.-G. Jahnke, V. Semkova, S. Haupt, M. Girard, M. Peschanski, O. Brustle, A.A. Robitzki, Impedimetric real-time monitoring of neural pluripotent stem cell differentiation process on microelectrode arrays, Biosens. Bioelectron. 86 (2016) 277–286, https://doi.org/10.1016/j.bios.2016.06.056.

[14] R. Szulcek, H.J. Bogaard, G.P.V.N. Amerongen, Electric cell-substrate impedance sensing for the quantification of endothelial proliferation, Barrier Funct. Motil. (2014) 1–12, https://doi.org/10.3791/51300.

[15] I.O. K'Owino, O.A. Sadik, Impedance spectroscopy: a powerful tool for rapid biomolecular screening and cell culture monitoring, Electroanalysis 17 (2019) 2101–2113, https://doi.org/10.1002/elan.200503371.

[16] J. Wegener, C.R. Keese, I. Giaever, Electric cell-substrate impedance sensing (ECIS) as a noninvasive means to monitor the kinetics of cell spreading to artificial surfaces, Exp. Cell Res. 259 (2000) 158–166, https://doi.org/10.1006/excr.2000.4919.

[17] T. Sun, S. Tsuda, K.-P. Zauner, H. Morgan, On-chip electrical impedance tomography for imaging biological cells, Biosens. Bioelectron. 25 (2010) 1109–1115, https://doi.org/10.1016/j.bios.2009.09.036.

[18] H. Wu, W. Zhou, Y. Yang, J. Jia, P. Bagnaninchi, Exploring the potential of electrical impedance tomography for tissue engineering applications, Materials (Basel) 11 (2018).

[19] H.S. Song, O.S. Kwon, J.-H. Kim, J. Conde, N. Artzi, 3D hydrogel scaffold doped with 2D graphene materials for biosensors and bioelectronics, Biosens. Bioelectron. 89 (2017) 187–200, https://doi.org/10.1016/j.bios.2016.03.045.
[20] B. Guo, L. Glavas, A.-C. Albertsson, Biodegradable and electrically conducting polymers for biomedical applications, Prog. Polym. Sci. 38 (2013) 1263–1286, https://doi.org/10.1016/j.progpolymsci.2013.06.003.
[21] K.F. Lei, Z.-M. Wu, C.-H. Huang, Impedimetric quantification of the formation process and the chemosensitivity of cancer cell colonies suspended in 3D environment, Biosens. Bioelectron. 74 (2015) 878–885, https://doi.org/10.1016/j.bios.2015.07.060.
[22] K.F. Lei, C.-H. Huang, N.-M. Tsang, Impedimetric quantification of cells encapsulated in hydrogel cultured in a paper-based microchamber, Talanta. 147 (2016) 628–633, https://doi.org/10.1016/j.talanta.2015.10.052.
[23] C. Canali, A. Heiskanen, H.B. Muhammad, P. Hoyum, F.-J. Pettersen, M. Hemmingsen, A. Wolff, M. Dufva, O.G. Martinsen, J. Emneus, Bioimpedance monitoring of 3D cell culturing–complementary electrode configurations for enhanced spatial sensitivity, Biosens. Bioelectron. 63 (2015) 72–79, https://doi.org/10.1016/j.bios.2014.07.020.
[24] Xueji Zhang, Huangxian Ju, Joseph Wang, H Zhang, J.B.T Ju, E.S. Wang (Eds.), Biosensors and their Biomedical Applications, Academic Press, San Diego, 2008, pp. xxi–xxii, , https://doi.org/10.1016/B978-012373738-0.50002-7.
[25] D. Birch, R.G. Diedrichsen, P.C. Christophersen, H. Mu, H.M. Nielsen, Evaluation of drug permeation under fed state conditions using mucus-covered Caco-2 cell epithelium, Eur. J. Pharm. Sci. (2018), https://doi.org/10.1016/j.ejps.2018.02.032.
[26] L.-Y. Luo, M.-X. Fan, H.-Y. Zhao, M.-X. Li, X. Wu, W.-Y. Gao, Pharmacokinetics and bioavailability of the isoflavones formononetin and ononin and their in vitro absorption in ussing chamber and Caco-2 cell models, J. Agric. Food Chem. 66 (2018) 12453, https://doi.org/10.1021/acs.jafc.8b05848.
[27] W. Neuhaus, A. Piontek, J. Protze, M. Eichner, A. Mahringer, E.-A. Subileau, I.-F.M. Lee, J.D. Schulzke, G. Krause, J. Piontek, Reversible opening of the blood-brain barrier by claudin-5-binding variants of Clostridium perfringens enterotoxin's claudin-binding domain, Biomaterials. 161 (2018) 129–143, https://doi.org/10.1016/j.biomaterials.2018.01.028.
[28] E. Van Rymenant, L. Abranko, S. Tumova, C. Grootaert, J. Van Camp, G. Williamson, A. Kerimi, Chronic exposure to short-chain fatty acids modulates transport and metabolism of microbiome-derived phenolics in human intestinal cells, J. Nutr. Biochem. 39 (2017) 156–168, https://doi.org/10.1016/j.jnutbio.2016.09.009.
[29] M. Natoli, B.D. Leoni, I. D'Agnano, F. Zucco, A. Felsani, Good Caco-2 cell culture practices, Toxicol. Vitr. 26 (2012) 1243–1246, https://doi.org/10.1016/j.tiv.2012.03.009.
[30] J. Fantini, B. Abadie, A. Tirard, L. Remy, J.P. Ripert, A. el Battari, J. Marvaldi, Spontaneous and induced dome formation by two clonal cell populations derived from a human adenocarcinoma cell line, HT29, J. Cell Sci. 83 (1986) 235–249.
[31] M. Natoli, B.D. Leoni, I. D'Agnano, M. D'Onofrio, R. Brandi, I. Arisi, F. Zucco, A. Felsani, Cell growing density affects the structural and functional properties of Caco-2 differentiated monolayer, J. Cell. Physiol. 226 (2011) 1531–1543, https://doi.org/10.1002/jcp.22487.
[32] S. Ferruzza, C. Rossi, M.L. Scarino, Y. Sambuy, A protocol for in situ enzyme assays to assess the differentiation of human intestinal Caco-2 cells, Toxicol. in Vitro 26 (2012) 1247–1251, https://doi.org/10.1016/j.tiv.2011.11.007.
[33] O.J. Myers, M. Anjanappa, C. Freidhoff, Designing piezoelectric interdigitated microactuators using finite element analysis, J. Mech. Des. 132 (2010) 61004–61011.
[34] M. Eichler, H.G. Jahnke, D. Krinke, A. Müller, S. Schmidt, R. Azendorf, A.A. Robitzki, A novel 96-well multielectrode array based impedimetric monitoring platform for comparative drug efficacy analysis on 2D and 3D brain tumor cultures, Biosens. Bioelectron. 67 (2015), https://doi.org/10.1016/j.bios.2014.09.049.
[35] H.-G. Jahnke, A. Braesigk, T.G.A. Mack, S. Ponick, F. Striggow, A.A. Robitzki, Impedance spectroscopy based measurement system for quantitative and label-free real-time monitoring of tauopathy in hippocampal slice cultures, Biosens. Bioelectron. 32 (2012) 250–258, https://doi.org/10.1016/j.bios.2011.12.026.
[36] J.E. Jackson, A User's Guide to Principal Components, J. Edward Jackson, 1991.
[37] J.M. Bland, D.G. Altman, Statistical methods for assessing agreement between two methods of clinical measurement, Lancet (London, England) 1 (1986) 307–310.
[38] P.F. Watson, A. Petrie, Method agreement analysis: a review of correct methodology, Theriogenology. 73 (2010) 1167–1179, https://doi.org/10.1016/j.theriogenology.2010.01.003.
[39] P. Schmiedlin-Ren, K.E. Thummel, J.M. Fisher, M.F. Paine, K.S. Lown, P.B. Watkins, Expression of enzymatically active CYP3A4 by Caco-2 cells grown on extracellular matrix-coated permeable supports in the presence of 1alpha,25-dihydroxyvitamin D3, Mol. Pharmacol. 51 (1997) 741–754.
[40] S. Ferruzza, C. Rossi, M.L. Scarino, Y. Sambuy, A protocol for differentiation of human intestinal Caco-2 cells in asymmetric serum-containing medium, Toxicol. Vitr. 26 (2012) 1252–1255, https://doi.org/10.1016/j.tiv.2012.01.008.
[41] K.A. Lentz, J. Hayashi, L.J. Lucisano, J.E. Polli, Development of a more rapid, reduced serum culture system for Caco-2 monolayers and application to the biopharmaceutics classification system, Int. J. Pharm. 200 (2000) 41–51, https://doi.org/10.1016/S0378-5173(00)00334-3.
[42] S. Tonello, N.F. Lopomo, M. Serpelloni, M. Serzanti, P. Dellera, E. Sardini, Preliminary study of inkjet printed sensors for monitoring cell cultures, Proc. Eng. 168 (2016) 578–581, https://doi.org/10.1016/j.proeng.2016.11.218.
[43] R. Ehret, W. Baumann, M. Brischwein, A. Schwinde, K. Stegbauer, B. Wolf, Monitoring of cellular behaviour by impedance measurements on interdigitated electrode structures, Biosens. Bioelectron. 12 (1997) 29–41, https://doi.org/10.1016/0956-5663(96)89087-7.
[44] B.-W. Chang, C.-H. Chen, S.-J. Ding, D.C.-H. Chen, H.-C. Chang, Impedimetric monitoring of cell attachment on interdigitated microelectrodes, Sensors Actuators B Chem. 105 (2005) 159–163, https://doi.org/10.1016/j.snb.2004.05.048.
[45] R. Igreja, C.J. Dias, Dielectric response of interdigital chemocapacitors: the role of the sensitive layer thickness, Sensors Actuators B Chem. 115 (2006) 69–78, https://doi.org/10.1016/j.snb.2005.08.019.
[46] M. Vakilian, B.Y. Majlis, Study of interdigitated electrode sensor for lab-on-chip applications, 2014 IEEE Int. Conf. Semicond. Electron, 2014, pp. 201–204, , https://doi.org/10.1109/SMELEC.2014.6920831.
[47] E.B. Secor, Principles of aerosol jet printing, Flex. Print. Electron. 3 (2018) 35002.
[48] E. Jabari, E. Toyserkani, Aerosol-jet printing of highly flexible and conductive graphene/silver patterns, Mater. Lett. 174 (2016) 40–43, https://doi.org/10.1016/j.matlet.2016.03.082.
[49] K. Benson, S. Cramer, H.-J. Galla, Impedance-based cell monitoring: barrier properties and beyond, Fluids Barriers CNS. 10 (2013) 5, https://doi.org/10.1186/2045-8118-10-5.
[50] D. Das, F.A. Kamil, K. Biswas, S. Das, Evaluation of single cell electrical parameters from bioimpedance of a cell suspension, RSC Adv. 4 (2014) 18178–18185, https://doi.org/10.1039/C4RA00400K.
[51] C.M. Lo, C.R. Keese, I. Giaever, Impedance analysis of MDCK cells measured by electric cell-substrate impedance sensing, Biophys. J. 69 (1995) 2800–2807, https://doi.org/10.1016/S0006-3495(95)80153-0.
[52] E. Urdapilleta, M. Bellotti, F.J. Bonetto, Impedance analysis of cultured cells: a mean-field electrical response model for electric cell-substrate impedance sensing technique, Phys. Rev. E Stat. Nonlinear Soft Matter Phys. 74 (2006) 41908, https://doi.org/10.1103/PhysRevE.74.041908.
[53] C. Xiao, B. Lachance, G. Sunahara, J.H.T. Luong, An in-depth analysis of electric cell-substrate impedance sensing to study the attachment and spreading of mammalian cells, Anal. Chem. 74 (2002) 1333–1339.
[54] B. Srinivasan, A.R. Kolli, M.B. Esch, H.E. Abaci, M.L. Shuler, J.J. Hickman, TEER measurement techniques for in vitro barrier model systems, J. Lab. Autom. 20 (2015) 107–126, https://doi.org/10.1177/2211068214561025.
[55] M. Amin, P.P. Dey, H. Badkoobehi, A complete electrical equivalent circuit model for biological cell, Proc. 7th WSEAS Int. Conf. Appl. Comput. Appl. Comput. Sci., World Scientific and Engineering Academy and Society (WSEAS), Stevens Point, Wisconsin, USA, 2008, pp. 343–348.
[56] J. Hickman, Transepithelial/endothelial electrical resistance (TEER) theory and applications for microfluidic body-on-a-chip devices, J. Rare Dis. Res. Treat. 1 (2016) 46–52, https://doi.org/10.29245/2572-9411/2016/3.1026.
[57] E. Latorre, S. Kale, L. Casares, M. Gómez-González, M. Uroz, L. Valon, R.V. Nair, E. Garreta, N. Montserrat, A. del Campo, B. Ladoux, M. Arroyo, X. Trepat, Active superelasticity in three-dimensional epithelia of controlled shape, Nature 563 (2018) 203–208, https://doi.org/10.1038/s41586-018-0671-4.